Batteries & Supercaps

Research Article
doi.org/10.1002/batt.202400558

Chemistry Europe
European Chemical Societies Publishing

www.batteries-supercaps.org

Constructing a Spider-Web Polymer Blocking Layer on Separator for the High-Loading Li-S Battery

Qian Zhang,[a] Jiajun Wan,[b] Qingping Gao,[a] and Jie Liu*[b]

The cycling performance of high-loading Li–S batteries is still puzzled by the serious shuttle effect of polysulfides. Modifying the commercial separator with polysulfide anchoring materials has been demonstrated as an economical and effective approach to block the polysulfide shuttle. Herein, a cobweb-like polymer polysulfide-blocking layer has been constructed via crosslinking between lithium polysilicate (LP) inorganic oligomer and tannic acid (TA) dendritic polymer. Owing to the strongly polar Si–O and Si=O bonds in LP, the spider-web polymer possesses robust affinity towards polysulfides, indicated by the theoretical calculations. Dendritic polymer TA as the skeleton contributes to effectively exposing the abundant polar functional groups to powerfully capture the polysulfides. As a result, the cycling stability of high-loading Li–S batteries has been obviously improved. The Li–S battery with sulfur loading of 3.44 mg cm^{-2} can stably cycle 100 cycles with a high capacity of 685.1 mAh g^{-1} and columbic efficiency of 99.82%. Even the sulfur loading increases to 7.15 mg cm^{-2}, the Li–S battery can still deliver a high areal capacity of 5.26 mAh cm^{-2} after 50 cycles.

Introduction

Li–S batteries possess high theoretical energy density of 2600 Wh kg^{-1} and attract broad attentions.[1–3] Furthermore, the sulfur active materials have the advantages of low cost and abundant resource. Therefore, Li–S batteries show great application prospect in the field of electric vehicles and smart power grids. However, for the sulfur cathode, heavy soluble polysulfide intermediates (Li_2S_x, $x \geq 4$) occur during cycling. Due to the weak interaction between commercial PP/PE separators and polysulfides, the polysulfides can easily diffuse to the anode side under concentration gradient and electric field, causing shuttle effect. The serious shuttle effect of the polysulfides leads to loss of active materials, corrosion of Li anode, and low coulombic efficiency.[4–6]

To suppress the shuttle effect, various host materials have been designed to constraint polysulfides within the cathode matrix, including porous carbon, metal compounds, and functional polymers.[7–11] Modifying the commercial separator as the polysulfide blocking layer is anther effective and economic strategy to enhance the electrochemical performance of Li–S batteries.[12–20] The ion shielding effect has been introduced into the functional separator, in which the negatively charged functional moiety of the composite separator can electrostatically repulse polysulfide anions (S_x^{2-}).[21,22] Conductive and nonpolar carbon materials were coated on the separator as the physical barrier, which can provide fast electron transfer to improve the redox dynamics of the polysulfides.[23] Polar functional materials with strong chemisorption effect towards polar polysulfides have also been demonstrated as promising separator modifying materials.[24,25] For example, we designed the multifunctional cation-vacancy-rich $ZnCo_2O_4$ (ZDZCO) polysulfide-blocking layer on PP separator.[15] DFT theoretical calculation indicates that the Zn vacancy in the subsurface layer provides enough space for the Li in Li_2S_x to penetrate into the surface and bind strongly to oxygen anions in the top layer. As a result, the ZDZCO-separator can effectively suppress the shuttle effect under an ultrahigh sulfur loading of 21.06 mg cm^{-2}. Organic polymers possess excellent flexibility and controllable structure and function, and thus are promising separator modification materials.[26–28] For example, a covalent organic framework (HUT9) has been synthesized on carbon nanotubes as the separator modification material, in which the disulfide bond could effectively capture soluble polysulfides to suppress the shuttle.[28] Therefore, the Li–S battery with sulfur loading of 4 mg cm^{-2} can reach an areal capacity of 3.4 mAh cm^{-2} after 50 cycles. Nonetheless, the inorganic modification materials are usually required additional binders to coat onto the separator, which not only increase the coating weight but also cover active sites. Organic polymer modification materials usually can not possess effective affinity towards polysulfides, epically under high sulfur loading.

Herein, we constructed a lithium polysilicate-tannic acid (LT) cobweb-like polymer polysulfide-blocking layer on the PP separator, which acts as the binder simultaneously. In the LT polysulfide-blocking layer, lithium polysilicate (LP) inorganic oligomer is rich in Si–O and Si=O bonds, which possess stronger polarity than that of C–O and C=O bonds in the organic polymers. While tannic acid (TA) is a dendritic polymer, which can effectively expose the abundant polar functional groups. Therefore, the LT spider-web blocking layer can show strong affinity towards polysulfides to block the polysulfide shuttle. As a result, when the sulfur loading is as high as

[a] Q. Zhang, Q. Gao
School of Chemistry and Engineering, Weifang Vocational College, Weifang 261108, China

[b] J. Wan, J. Liu
Youth Innovation Team of Shandong Higher Education Institutions, College of Chemical Engineering, Qingdao University of Science and Technology, Qingdao 266042, China
E-mail: jie.liu@qust.edu.cn

Research Article
doi.org/10.1002/batt.202400558
Chemistry Europe
European Chemical Societies Publishing

7.15 mg cm^{-2}, the Li–S battery with LT-separator can still deliver a high areal capacity of 5.26 mAh cm^{-2} after 50 cycles.

Results and Discussion

The lithium polysilicate (LP) is rich in polar Si–O and Si=O bonds (Figure 1a), which make it a convenient platform for chemical interactions with the polar groups/molecules. Tannic acid (TA) is a dendritic polymer (Figure 1b), which contains abundant polar oxygen-containing functional groups (e.g., –OH, –COOR).[29–31] After mixing LP with TA, a crosslinking effect can occur between Si–O/Si=O groups and –COOR/–OH groups to form the LT spider-web polymer composite, as shown in Figure 1c. To demonstrate the crosslinking reaction between LP and TA, FTIR spectra of LP, TA, and LT are obtained and shown in Figure 1d. The LP shows the bond at 1183.5, 1065.9, and 792.2 cm^{-1} corresponding to Si–O–Si and O–Si–O stretching vibrations.[32] The TA shows the stretching vibration of the phenolic hydroxyl group at 3305.1 cm^{-1} and the C=O stretching vibration of the ester group at 1724.5 cm^{-1}.[33,34] After crosslinking, the vibration peaks show obvious shift, indicating that a chemical interaction occurs between LP and TA.

To prepare the functional separator, LT network polymer acting as both binder and functional layer is coated on the commercial PP separator. Super P conductive carbon is added into the functional coating, which makes the functional separator as the upper current collector. Figure 2 shows the surface morphology of the LT-separator and the corresponding element mappings. One can observe that the Si, O, and Li elements are dispersed over the separator. Therefore, the LT

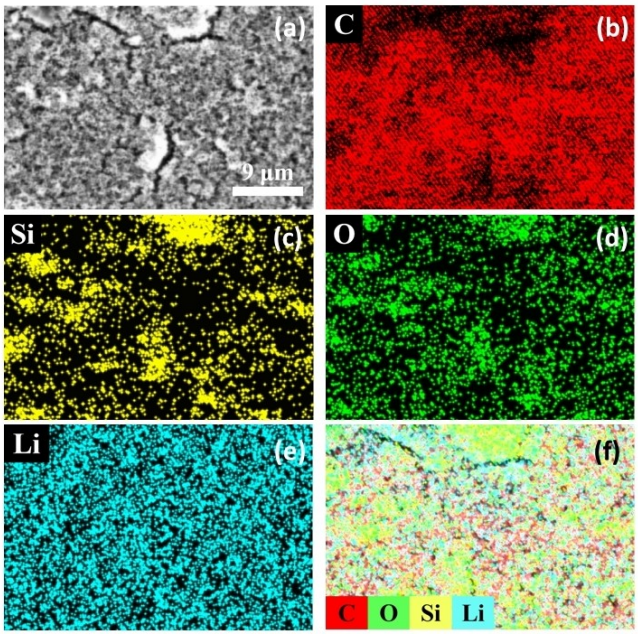

Figure 2. (a) The top-view SEM image of the LT-separator, and (b-f) the corresponding element distribution of C, Si, O, and Li.

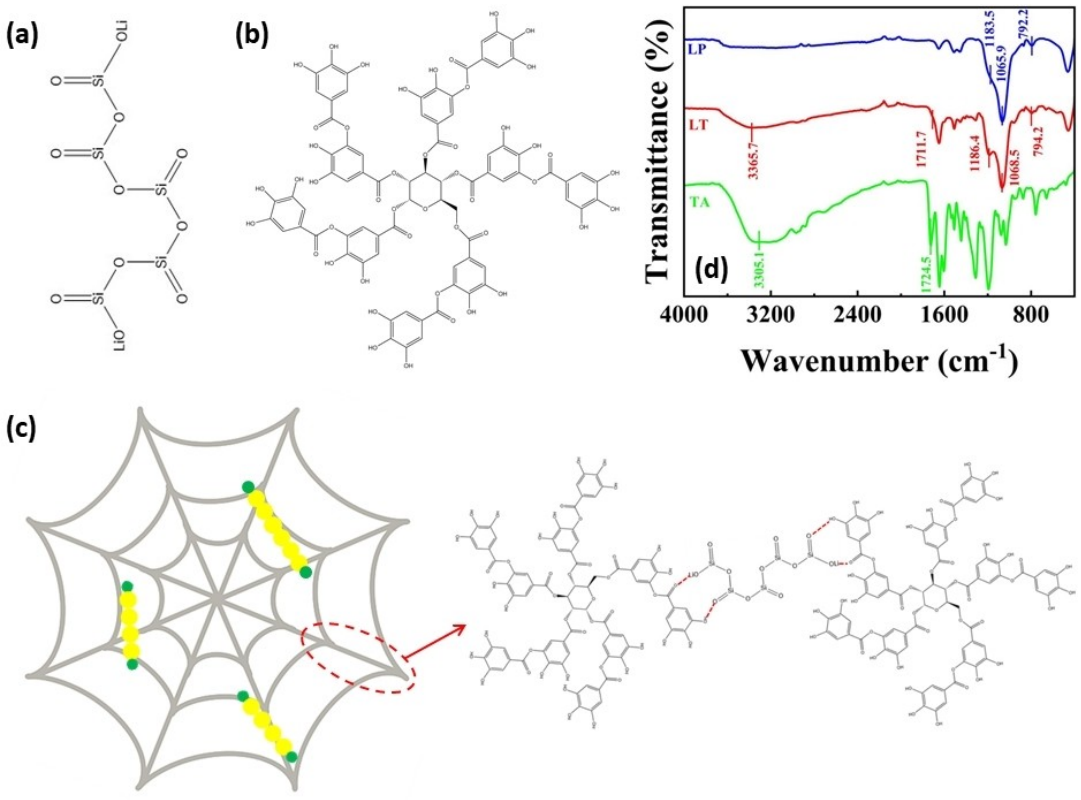

Figure 1. The molecular structure of (a) lithium polysilicate (LP) and (b) tannic acid (TA), (c) the schematic diagram of the LT spider-web polymer formed via crosslinking between LP and TA, (d) FTIR spectra of LP, TA, and LT.

network functional layer on PP separator can effectively absorb polysulfides to block the shuttle effect. Moreover, the evenly dispersed super P conductive carbon (Figure 2b) can ensure fast electronic transfer to the adsorbed polysulfides. As a result, the adsorbed polysulfides can continue to transform to the final product, which improves the sulfur utilization rate.

To show the effect of the LT-separator on the cycling stability of Li–S battery, galvanostatic charge-discharge tests are carried out. As shown in Figure 3a, the Li–S battery with LT-separator can deliver a high capacity of 500.4 mAh g^{-1} after a long cycling of 1000 cycles at 0.5 C. While the Li–S battery with PP-separator shows a low capacity of 348.2 mAh g^{-1} after 1000 cycles. To exclude the effect of super P on the cycling stability, the Li–S battery with super P-separator is also compared. And it only can give a capacity of 388.4 mAh g^{-1} after 1000 cycles. These results demonstrate the improved cycling stability of the Li–S battery is mainly due to the LT spider-web polymer blocking layer. To achieve high energy density, high-loading Li–S battery is crucial.[35–38] Therefore, high-loading Li–S battery with LT-separator is achieved. When the sulfur loading increases to 3.44 mg cm^{-2}, the Li–S battery with LT-separator can stably cycle 100 cycles with a high capacity of 685.1 mAh g^{-1} and coulombic efficiency of 99.82 % (Figure 3b). However, the Li–S battery with commercial PP-separator shows severe shuttle effect and cell failure after only 55 cycles, as shown in Figure 3b and c. Even when the sulfur loading is as high as 7.15 mg cm^{-2}, the Li–S battery with LT-separator can still deliver a high areal capacity of 5.26 mAh cm^{-2} after 50 cycles, indicating the high practical application potential.

Figure 3e also compares the rate property of the high-loading Li–S batteries using different separators. It shows that the high-loading Li–S battery using LT-separator displays superior rate property. When the current density increases to 1.6 mA cm^{-2}, it can still deliver a high capacity of 679.8 mAh g^{-1}. Nevertheless, the Li–S battery with PP-separator shows a low capacity of only 208.5 mAh g^{-1}. Figure 3f shows the charge-discharge curves of the high-loading Li–S battery using LT-separator under different current density. Even the current density increases to 1.6 mA cm^{-2}, the high-loading Li–S battery using LT-separator still retains the two-discharge-platform characteristic. However, the high-loading Li–S battery using PP-separator shows large electrode polarization, leading to the low discharge capacity (Figure 3g). The enhanced redox dynamic of high-loading Li–S battery using LT-separator can be attributed to the improved wettability of the functional separator (Figure 4a and b). The LT polymer contains abundant polar functional groups, which can form strong affinity with the polar solvent to improve the wettability and thusboost the Li^+ ion transfer (Figure 4c). As the electronegative functional groups can form effective affinity towards Li^+ ions, the Li^+ transference number can also be improved when the LT-separator is applied (Figure 4d–f).

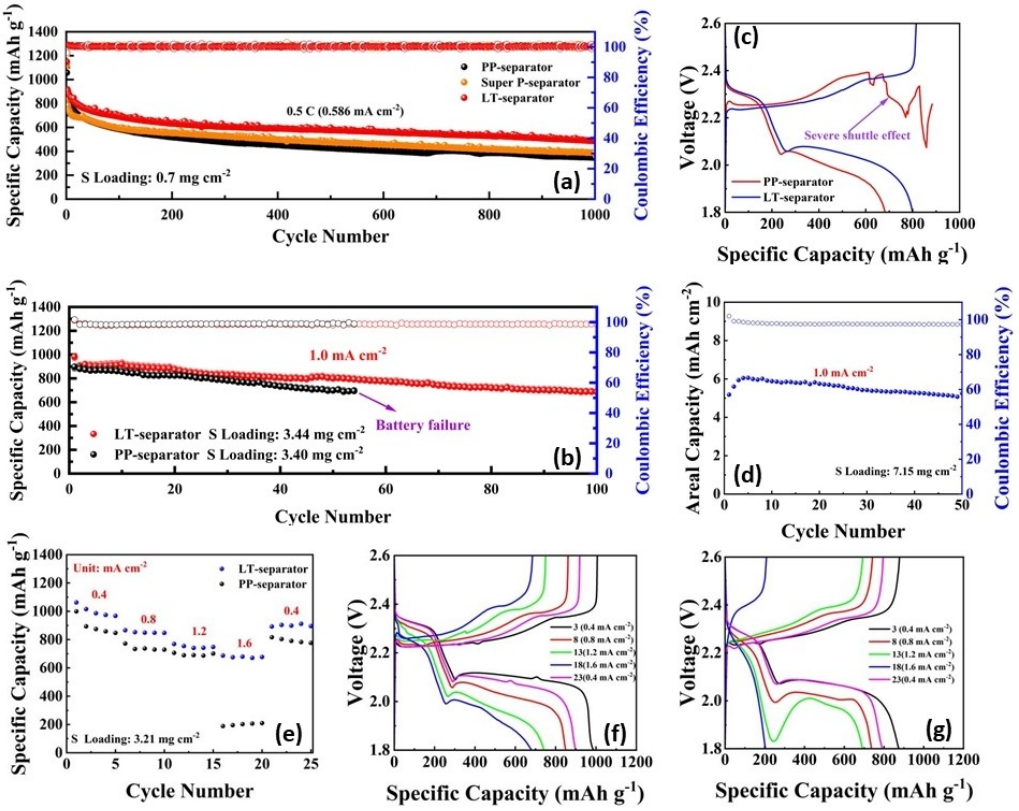

Figure 3. (a) The cycling performance of the Li–S batteries using different separators under 0.5 C, (b) the cycling performance and (c) the charge-discharge curves at the 55th cycle of the high-loading Li–S batteries using LT-separator and PP-separator, (d) the cycling performance of the Li–S battery using LT-separator under the sulfur loading of 7.15 mg cm^{-2}, (e-g) the rate property and corresponding charge-discharge curves of the high-loading Li–S batteries using LT-separator and PP-separator.

Research Article
doi.org/10.1002/batt.202400558
Chemistry Europe
European Chemical Societies Publishing

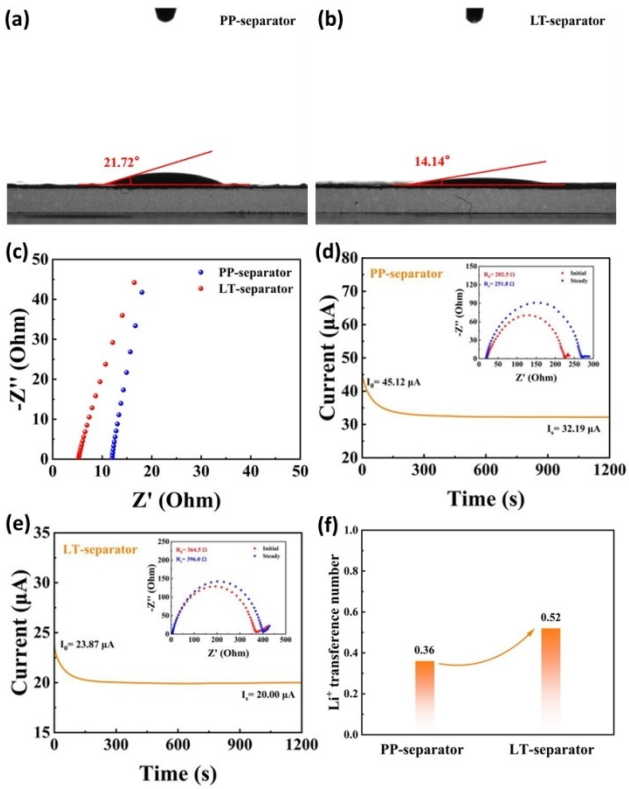

Figure 4. The contact angle of the electrolyte on (a) PP-separator and (b) LT-separator, (c) the Nyquist plots of occluded cells consisting of stainless steel//separator//stainless steel, the CA curve of the Li//Li symmetric cell under a polarization potential of 10 mV with (d) PP-separator and (e) LT-separator (inset: Nyquist plots of the cell before and after polarization), (f) the corresponding Li^+ transference number.

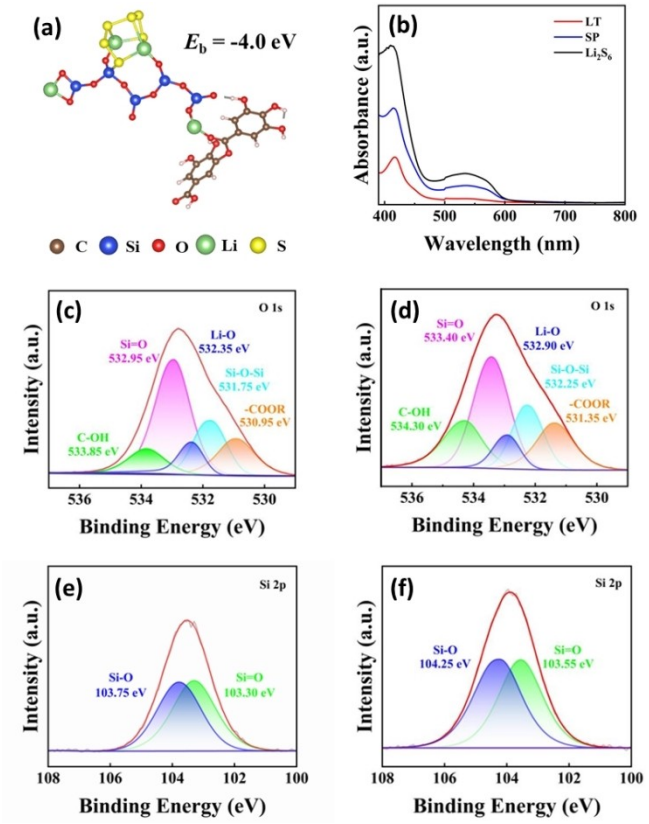

Figure 5. (a) The adsorption structure of Li_2S_6 on LT polymer and corresponding binding energy, (b) the UV-vis absorption spectra of the Li_2S_6 solutions after soaking super P (SP) and LT, (c, d) the O 1s XPS spectra of LT polymer before and after adsorbing Li_2S_6, (e, f) the Si 2p XPS spectra of LT polymer before and after adsorbing Li_2S_6.

The rich polar functional groups in LT spider-web polymer can also powerfully anchor polar polysulfides to dramatically hinder the shuttle effect. DFT theoretical simulation is applied to demonstrate the strong affinity between LT network polymer and polysulfides (Li_2S_6). From Figure 5a, one can observe that the Li atom in Li_2S_6 tends to bond with O atom in Si=O, while the S atom tends to bond with Si atom in Si=O. Therefore, the high binding energy (−4.0 eV) between LT spider-web polymer and Li_2S_6 can be achieved. This binding energy is obviously stronger than the organic polymers (typically $<$2.0 eV).[39,40] The UV-vis absorption spectra of the Li_2S_6 solutions can clearly demonstrate the strong polysulfide adsorption capability of the LT polymer, in which the peak intensity of Li_2S_6 obviously decreases after soaking LT polymer (Figure 5b). The XPS spectra of the LT polymer before and after adsorbing Li_2S_6 are compared in Figure 5c–f. Before adsorbing Li_2S_6, the O 1s XPS spectrum of LT polymer shows the bonds at 533.85, 532.95, 532.35, 531.75, and 530.95 eV, corresponding to the C–OH, Si=O, Li–O, Si–O–Si, and –COOR.[41,42] While after adsorbing Li_2S_6, these bonds shift to higher binding energy at 534.30, 533.40, 532.90, 532.25, and 531.35 eV, respectively. In Si 2p XPS spectrum, the bonds at 103.75 and 103.30 eV can be attributed to Si–O and Si=O,[41] and they shift to 104.25 and 103.55 eV after adsorbing Li_2S_6. These results obviously indicate the electron transfer from the electronegative O atom in the spider-web polymer to the Li^+ ions in Li_2S_6 and the strong chemical interactions occur.

To visually show the suppressed shuttle effect by the LT spider-web coating under electric field and concentration gradient, in-situ cells are assembled. From Figure 6a and b, it can be observed that the Li–S cell with LT-coating displays longer upper discharge platform. This indicates more polysulfides can be constrained in the sulfur cathode side to participate in electrochemical reactions. The digital photos of the in-situ cell at different discharge states in Figure 6c and d can visually display the solution rate of polysulfides into electrolyte. When the sulfur cathode without the LT-coating is used in the in-situ cell, the electrolyte quickly becomes dark yellow only after discharging for 15 min. While the sulfur cathode with LT-coating is applied, the electrolyte remains almost colorless until 45 min, suggesting less polysulfides in the electrolyte. The surface morphology of the Li anodes after cycling is also checked. Figure 7a and b shows the initial Li anode is smooth. After 50 cycles, the Li anode from the Li–S battery with PP-separator is very rough due to the severe corrosion and passivation by the polysulfides (Figure 7c and d). However, the Li anode from the Li–S battery with LT-separator

Research Article
doi.org/10.1002/batt.202400558
Chemistry Europe
European Chemical Societies Publishing

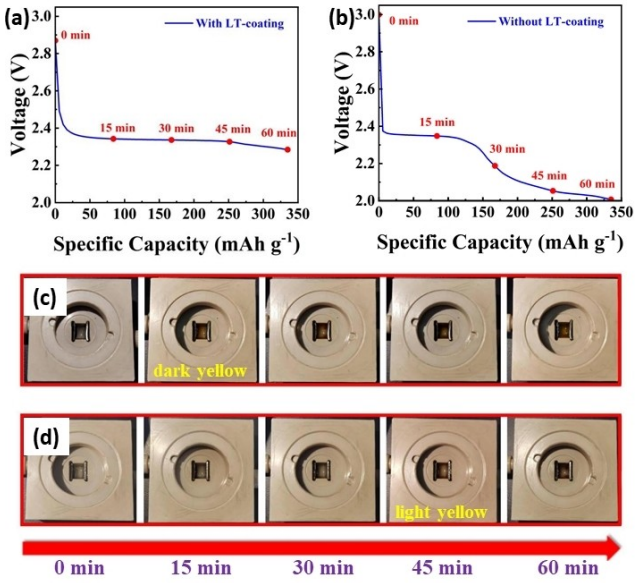

Figure 6. The charge-discharge curves of the in-situ cells using sulfur electrodes (a) with LT-coating and (b) without LT-coating, (c) the digital photos of the in-situ cell using sulfur electrode without LT-coating at different discharge states, (d) the digital photos of the in-situ cell using sulfur electrode with LT-coating at different discharge states.

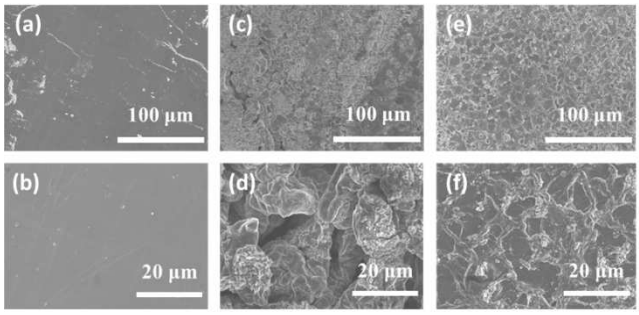

Figure 7. The SEM images of the Li anodes (a, b) before cycling, (c, d) after 50 cycles with PP-separator, (e, f) after 50 cycles with LT-separator.

is relative flat, indicting the suppressed polysulfide shuttle by the LT-coating (Figure 7e and f).

Conclusions

To suppress the shuttle effect in high-loading Li–S battery, a LT cobweb-like polymer polysulfide-blocking layer has been constructed on PP separator via blade-coating method. In LT network, lithium polysilicate (LP) inorganic oligomer with rich Si–O and Si=O bonds contributes to robust affinity towards polysulfides, owing to its stronger polarity than organic polymers containing C–O and C=O bonds. The dendritic polymer tannic acid (TA) as the skeleton of the cobweb-like polymer helps to suppress the agglomeration and expose the adsorption active sites. The robust chemisorption effect between LT network polymer and polysulfides has been demonstrated by the DFT calculation, UV-vis absorption spectra, and XPS spectra. And the polysulfide-blocking effect of the LT blocking layer can be visually demonstrated by the color change of electrolyte during discharge and SEM images of the cycled Li anodes. As a result, the cycling stability of high-loading Li–S batteries have been obviously improved, indicating the practical application potential.

Methods

Materials

Tannic acid (TA, AR) and tetrahydrofuran (THF, AR) were purchased from Macklin (Shanghai) Biochemical Technology Co., LTD. Sulfur powder (S, AR) and lithium sulfide (Li_2S, AR) were purchased from Aladdin (China) Co., LTD. Lithium polysilicate (LP, 20 wt% in H_2O) was from Sigma-Aldrich (Shanghai) Trading Co., LTD. Super P (SP, battery level) was from TIMCAL (Switzerland) Co., LTD. Ketjen black (KB, battery level) was from LION (Japan) Co., LTD. Polyvinylidene fluoride (PVDF, battery level) was purchased from Kejing (Hefei) Electronic Technology Co., LTD. Li–S electrolyte (LS002) was purchased from Duoduo Chemical (Suzhou) Technology Co., LTD. All of the above reagents were used directly without further purification.

Characterization

Scanning electron microscopy (SEM, Hitachi Regulus 8100) was used to characterize the surface micromorphology of the samples. Elemental mapping was obtained on an EDAX Genesis energy dispersive X-ray fluorescence spectrometer. FTIR spectra in the range of 4000–400 cm^{-1} were measured using Fourier transform infrared spectroscopy (FTIR, Thermo Scientific Nicolet iS20). The UV-vis spectra of Li_2S_6 solutions after adsorption experiments were measured by UV-vis spectrophotometer (Metash UV-8000). The XPS spectra of LT before and after adsorption of Li_2S_6 were analyzed with X-ray photoelectron spectroscopy (XPS, ESCALAB XI+).

Preparation of Sulfur Electrode

The sulfur powder was ground with super P with a mass ratio of 6:4, then transferred into a 100 mL stainless steel autoclave lined with PTFE and heated at 155 °C for 12 h to obtain S/super P composite material. The cathode slurry was prepared by uniformly mixing 80 wt% S/super P composite, 10 wt% Ketjen black (KB), and 10 wt% PVDF binder in NMP. Afterward, the mixed slurry was blade-coated on carbon coated aluminum foil and dried at 60 °C in a vacuum drying oven for 12 h. The sulfur loading is about 0.7 mg cm^{-2}. The high-loading electrode was prepared by coating the slurry uniformly onto the carbon paper, and the mass loading of sulfur was controlled in the range of 3.00 mg cm^{-2} to 7.15 mg cm^{-2}.

Preparation of Functional Separator

LP/TA (7:3 in weight) was evenly mixed with super P in NMP at a mass ratio of 6:4, and then the slurry was evenly coated on the commercial Celgard 2325 separator. The modified separator was dried by vacuum drying at 60 °C for 12 h. The mass loading of the functional coating is typically 0.2 mg cm^{-2}. In order to explore the influence of super P, the super P-separator was also obtained using super P and PVDF binder under the mass ratio of 9:1.

Electrochemical Performance Tests

When the sulfur loading was 0.7 mg cm^{-2}, the sulfur cathode, the functional separator, and the lithium anode are assembled into the CR2016 cell in a glove box filled with argon gas. The 30 μL of the electrolyte containing 1 M LiTFSI in a 1,2-dimethoxyethane and 1,3-dioxolame (1:1 v/v) mixed solvent with 2 wt% $LiNO_3$ was added to the cell. The assembled battery was tested on a LAND battery test system at room temperature (25 °C). When the sulfur loading was 3.00 mg cm^{-2} to 7.15 mg cm^{-2}, the amount of electrolyte was 20 μL mg^{-1}, and the CR2032 coin cell was used.

To visually observe the shuttle effect of polysulfides, in-situ cell was assembled. We firstly prepared a sulfur cathode containing 80 wt% S/super P composite, 10 wt% KB and 10 wt% PVDF binder. After that, LT with super P at a mass ratio of 6:4 were evenly coated on the sulfur cathode as the blocking layer. The in-situ cell (Gaoshiruilian (Tianjin) Photoelectric Technology Co., LTD. Model 19004) was assembled using a sulfur cathode with/without LT-coating (1 cm×1 cm) and a lithium anode (1 cm×1 cm). The in-situ cell was tested on the LAND test system for 1 h at a current density of 0.2 C.

Polysulfide Adsorption Experiment

0.1 M Li_2S_6 solution was prepared by mixing Li_2S and sulfur powders in 6 mL tetrahydrofuran (THF) with a molar ratio of 1:5, followed by stirring and heating at 65 °C for 48 h. Then, 50 mL of 3 mM diluent was prepared for the polysulfide adsorption experiment. LT and super P were evenly mixed in NMP at a ratio of 6:4 and dried in the oven at 60 °C. Then 160 mg of the LT/super P powders were added into 3 mM Li_2S_6 solution for 24 h, and the supernatant was detected by UV-vis spectrophotometer to quantitatively determine the residual amount of Li_2S_6 in the solution after adsorption test.

DFT Calculation

Density functional theory (DFT) calculation was carried out using the Projector-Augmented Wave (PAW) method as implemented in the Vienna Ab Initio Simulation Package (VASP).[43] The Perdew-Burke-Erzenhoff (PBE)[44] form of the generalized gradient approximation (GGA) was employed to describe exchange and correlation effects. A Gamma point mesh, an energy cutoff of 500 eV as well as an energy convergence criterion of 0.0001 eV have been used for the calculation.

Acknowledgements

Q. Zhang and J. Wan contributed equally. This study was financially supported by the Youth Innovation Team Project of Shandong Higher Education Institutions (2022KJ309), the Weifang Science and Technology Development Programme Project (2022GX020 and 2022GX021), the National Natural Science Foundation of China (22005169), the Natural Science Foundation of Shandong Province (ZR2020QB121).

Conflict of Interests

The authors declare no conflict of interest.

Data Availability Statement

Data sharing is not applicable to this article as no new data were created or analyzed in this study.

Keywords: Li–S battery · Functional separator · High loading · Shuttle effect · Network polymer

[1] G. He, X. Ji, L. Nazar, *Energy Environ. Sci.* **2011**, *4*, 2878.
[2] S. H. Chung, C. H. Chang, A. Manthiram, *Energy Environ. Sci.* **2016**, *9*, 3188.
[3] J. Guo, Q. Yang, Y. Dou, X. Ba, W. Wei, J. Liu, *Energy Environ. Sci.* **2024**, *17*, 1695.
[4] M. Zhao, B. Q. Li, X. Q. Zhang, J. Q. Huang, Q. Zhang, *ACS Cent. Sci.* **2020**, *6*, 1095.
[5] Y. Wang, Z. Deng, J. Huang, H. Li, Z. Li, X. Peng, Y. Tian, J. Lu, H. Tang, L. Chen, Z. Ye, *Energy Storage Mater.* **2021**, *36*, 466.
[6] C. Kensy, F. Schwotzer, S. Dörfler, H. Althues, S. Kaskel, *Batteries & Supercaps* **2021**, *4*, 823.
[7] R. Wang, J. Yang, X. Chen, Y. Zhao, W. Zhao, G. Qian, S. Li, Y. Xiao, H. Chen, Y. Ye, G. Zhou, F. Pan, *Adv. Energy Mater.* **2020**, *10*, 1903550.
[8] X. Gu, H. Li, H. Wen, Y. Zhou, H. Kang, H. Liao, M. Gao, Y. Wang, L. Deng, X. Yi, X. Liu, *J. Mater. Sci.* **2020**, *55*, 1136.
[9] X. Wang, Y. Yang, C. Lai, R. Li, H. Xu, D. H. S. Tan, K. Zhang, W. Yu, O. Fjeldberg, M. Lin, W. Tang, Y. S. Meng, K. P. Loh, *Angew. Chem. Int. Ed.* **2021**, *60*, 11359.
[10] L. Zhou, D. L. Danilov, R. A. Eichel, P. H. L. Notten, *Adv. Energy Mater.* **2021**, *11*, 2001304.
[11] S. Zhao, X. Qian, L. Jin, B. Li, *Chem. Eur. J.* **2024**, *30*, e202401124.
[12] B. Guan, Y. Zhang, L. Fan, X. Wu, M. Wang, Y. Qiu, N. Zhang, K. Sun, *ACS Nano* **2019**, *13*, 6742.
[13] S. Xia, J. Song, Q. Zhou, L. Liu, J. Ye, T. Wang, Y. Chen, Y. Liu, Y. Wu, T. Ree, *Adv. Sci.* **2023**, *10*, 2301386.
[14] M. Waqas, Y. Niu, M. Tang, Y. Pang, S. Ali, Y. Dong, W. Lv, W. He, *Energy Storage Mater.* **2024**, *72*, 103682.
[15] Z. Li, Q. Zhang, L. Hencz, J. Liu, P. Kaghazchi, J. Han, L. Wang, S. Zhang, *Nano Energy* **2021**, *89*, 106331.
[16] W. Wang, M. Hou, F. Han, D. Yu, J. Liu, Q. Zhang, F. Yu, L. Wang, M. He, *J. Energy Chem.* **2023**, *82*, 581.
[17] X. Guan, Y. Zhao, H. Pei, M. Zhao, Y. Wang, X. Zhou, M. G. Mohamed, S. W. Kuo, Y. Ye, *Chem. Eng. J.* **2023**, *473*, 144733.

[18] Y. Yang, B. Sun, Z. Sun, J. Xue, J. He, Z. Wang, K. Sun, Z. Sun, H. K. Liu, S. X. Dou, *Coordin. Chem. Rev.* **2024**, *510*, 215836.
[19] C. Chen, Q. Jiang, H. Xu, Y. Zhang, B. Zhang, Z. Zhang, Z. Lin, S. Zhang, *Nano Energy* **2020**, *76*, 105033.
[20] Y. Li, J. Liu, X. Wang, X. Zhang, N. Chen, L. Qian, Y. Zhang, X. Wang, Z. Chen, *Small Sci.* **2023**, *3*, 2300045.
[21] J. Q. Huang, Q. Zhang, H. J. Peng, X. Y. Liu, W. Z. Qian, F. Wei, *Energy Environ. Sci.* **2014**, *7*, 347.
[22] Y. M. Kwon, J. Kim, K. Y. Cho, S. Yoon, *J. Energy Chem.* **2021**, *60*, 334.
[23] J. Balach, T. Jaumann, M. Klose, S. Oswald, J. Eckert, L. Giebeler, *Adv. Funct. Mater.* **2015**, *25*, 5285.
[24] C. Li, R. Liu, Y. Xiao, F. Cao, H. Zhang, *Energy Storage Mater.* **2021**, *40*, 439.
[25] S. Li, W. Zhang, J. Zheng, M. Lv, H. Song, L. Du, *Adv. Energy Mater.* **2021**, *11*, 2000779.
[26] P. T. Dirlam, R. S. Glass, K. Char, J. Pyun, *J. Polym. Sci. Part A: Polym. Chem.* **2017**, *55*, 1635.
[27] N. Batyrgali, Y. Yerkinbekova, N. Tolganbek, S. Kalybekkyzy, Z. Bakenov, A. Mentbayeva, *ACS Appl. Energy Mater.* **2023**, *6*, 588.
[28] M. Li, G. Yan, P. Zou, H. Ji, H. Wang, Z. Hu, Z. Yang, Y. Feng, H. Ben, X. Zhang, *ACS Sustainable Chem. Eng.* **2022**, *10*, 13638.
[29] L. Yang, Y. Wang, Q. Li, Y. Li, Y. Chen, Y. Liu, Z. Wu, G. Wang, B. Zhong, Y. Song, W. Xiang, Y. Zhong, X. Guo, *Nanoscale* **2021**, *13*, 5058.
[30] H. Zhang, C. Lin, X. Hu, B. Zhu, D. Yu, *ACS Appl. Mater. Interfaces* **2018**, *10*, 12708.
[31] W. Yan, M. Shi, C. Dong, L. Liu, C. Gao, *Adv. Colloid Interface Sci.* **2020**, *284*, 102267.
[32] M. S. Pathak, N. O. Gopal, N. Singh, M. Mohapatra, J. L. Rao, J. K. Lee, V. Singh, *J. Non-Cryst. Solids* **2018**, *500*, 266.
[33] M. Hou, J. Feng, F. Wang, W. Wang, Z. Li, J. Liu, F. Yu, L. Wang, *ACS Appl. Energy Mater.* **2022**, *5*, 13580.
[34] B. Muhoza, S. Xia, X. Zhang, *Food Hydrocoll.* **2019**, *97*, 10517.
[35] W. Wu, X. Li, L. Liu, X. Zhu, Z. Guo, W. Guo, Q. Han, J. He, Y. Zhao, *J. Mater. Chem. A* **2022**, *10*, 1433.
[36] Y. Feng, G. Wang, J. Ju, Y. Zhao, W. Kang, N. Deng, B. Cheng, *Energy Storage Mater.* **2020**, *32*, 320.
[37] R. Guo, Y. Yang, X. L. Huang, C. Zhao, B. Hu, F. Huo, H. K. Liu, B. Sun, Z. Sun, S. X. Dou, *Adv. Funct. Mater.* **2024**, *34*, 2307108.
[38] M. Wang, L. Fan, X. Sun, B. Guan, B. Jiang, X. Wu, D. Tian, K. Sun, Y. Qiu, X. Yin, Y. Zhang, N. Zhang, *ACS Energy Lett.* **2020**, *5*, 3041.
[39] J. Jian, Q. Chen, H. Sun, R. Li, Y. Hou, Y. Liu, J. Liu, H. Xie, J. Zhu, *J. Energy Chem.* **2024**, *97*, 228.
[40] T. Zhang, R. Mao, W. Jiang, B. Li, Z. Song, S. Liu, X. Jian, F. Hu, *Nano Energy* **2023**, *114*, 108603.
[41] F. Wang, Q. Zhang, Z. Liu, M. Hou, Z. Li, J. Liu, R. Wang, L. Wang, *J. Colloid Interface Sci.* **2023**, *629*, 1045.
[42] C. Liao, Q. Xu, C. Wu, D. Fang, S. Chen, S. Chen, J. Luo, L. Li, *J. Mater. Chem. A* **2016**, *4*, 17215.
[43] E. Blöchl, *Phys. Rev. B* **1994**, *50*, 17953.
[44] J. P. Perdew, K. Burke, M. Ernzerhof, *Phys. Rev. Lett.* **1996**, *77*, 3865.

Manuscript received: August 21, 2024
Revised manuscript received: September 16, 2024
Version of record online: October 30, 2024